Tetrakis(ferrocenylethynyl)ethene:synthesis, spectro)electrochemical and quantum chemical characterisation

Tetra(ferrocenylethynyl)ethene: Synthesis, (Spectro)electrochemical and Quantum Chemical Characterisation

Kevin B. Vincent,[a] Josef B. G. Gluyas,[b] Simon Gückel,[c] Qiang Zeng,[d,e] Frantisek Hartl,*[,d] Martin Kaupp,*[,c] Paul J. Low*[,b]

[a] *Department of Chemistry, Durham University, South Rd, Durham, DH1 3LE, UK*

[b] *School of Chemistry and Biochemistry, University of Western Australia, 35 Stirling Highway, Crawley 6009, WA, Australia.*

[c] *Technische Universität Berlin, Institut für Chemie Sekr. C7, Strasse des 17. Juni 135, 10623 Berlin, Germany.*

[d] *Department of Chemistry, University of Reading, Whiteknights, Reading, RG6 6AH, UK*

[e] *School of Chemistry and Chemical Engineering, South China University of Technology, Guangzhou 510640, PR China*

** Corresponding authors:*

PJL: paul.low@uwa.edu.au (t) +61 (08) 6488 3045

MK: martin.kaup@tu-berlin.de (t) +49 30 314 79682

FH: f.hartl@reading.ac.uk (t) +44 (0) 118 378 7695

ABSTRACT

Tetra(ferrocenylethynyl)ethene (**1**) has been prepared in four steps from ethynyl ferrocene (**2**). In a dichloromethane solution containing 10^{-1} M NBu_4PF_6, only a single oxidation process is observed by cyclic voltammetry, corresponding to the independent oxidation of the four ferrocenyl moieties. However, in dichloromethane containing 10^{-1} M $NBu_4BAr^F{}_4$ electrolyte, where $[BAr^F{}_4]^-$ is the weakly associating anion $[B\{C_6H_3(CF_3)_2\text{-}3,5\}]^-$, four distinct oxidation processes are resolved, although further spectroelectrochemical investigation revealed essentially no through bond interaction between the individual ferrocene moieties. Quantum chemical treatment of **1** identified several energetic minima corresponding to different relative orientations of the ferrocene moieties and the plane of the all-carbon bridging fragment. Further computational investigation of the corresponding monocation $[\mathbf{1}]^+$ supported the notion of charge localisation with no evidence for significant through bond electronic interactions.

Keywords: Ferrocene, Quantum Cellular Automata, Spectroelectrochemistry, DFT

1. INTRODUCTION

Molecular compounds that feature multiple, identical redox sites related by some element of symmetry, and which localize charge upon changes to the oxidation states of the redox centers are of interest as data elements and logic systems through the Quantum-dot Cellular Automata (QCA) concept [1] [2-5] [6], charge storage and memory applications [7]. The well-behaved redox chemistry of ferrocene derivatives

has led to interest in molecules containing more than two ferrocene units around a common core, such as 1,3,5-tris(ferrocenylethynyl)benzene [8,9], tetraferrocenyl(nickel dithiolene) [10] and hexakis(ferrocenylethynyl)benzene [11,12], and the electronic structures of the mixed-valence compounds derived from them. For example, the mono- and di-cations derived by one or two-electron oxidation of $\{CpFe(\eta^5\text{-}C_5H_4)\}_4(\eta^4\text{-}C_4)CoCp$ have been characterised as Class II and Class II-III mixed valence species based on the solvatochromic properties of the IVCT band, IR and Mössbauer spectroscopy.[6] The metal-free porphyrin bridged tetraferrocene complex 5,10,15,20-tetraferrocenylporphyrin (H_2TFcP) exhibits four independent one-electron oxidation waves in a 0.05 M $NBu_4[B(C_6F_5)_4]$ *ortho*-dichlorobenzene or CH_2Cl_2 solution, with comprehensive spectroscopic analysis leading to description of $[H_2TFcP]^{n+}$ (n = 1, 2, 3) as weakly coupled (Class II) mixed valence species, with coupling terms H_{ab} derived from the classical Hush expressions of the order of 550 – 1150 cm^{-1}.[V.N. Nemykin, G.T. Rohde, C.D. Barrett, R.G. Hadt, C. Bizzarri, P. Galloni, V. Floris, I. Nowik, R.H. Herber, A.G. Marrani, R. Zanoni, N.M. Loim, J. Am. Chem. Soc. 131 (2009) 14969-14978] Analogous transition metal porphyrin-bridged tetraferrocenyl complexes behave similarly.[G.T. Rohde, J.R. Sabin, C.D. Barrett, V.N. Nemykin, New J. Chem., 35 (2011), 1440-1448]

In looking to extend such studies, the cross-conjugated 1,1,2,2-tetraethynylethene can be identified as a possible bridge structure capable of linking multiple redox-active sites to a common, conjugated core. The synthetic chemistry of this carbon-rich motif has been well established [13,14] and hence tetra(ferrocenylethynyl)ethene (**1**) was envisioned as a potential target compound. This paper describes the synthesis of **1**, the electrochemical and spectroelectrochemical (IR, UV-vis-NIR) response of this unusually conjugated multi-ferrocenyl redox system, and a description of the

electronic structure from quantum chemical (BLYP35-D3/def2-TZVP/COSMO(CH_2Cl_2)) calculations.

2. RESULTS AND DISCUSSION

2.1 Synthesis Complex **1**, incorporating four ferrocenyl moieties around a 1,1,2,2-tetraethenylethyne core, was synthesised according to Scheme 1. The intermediates in the synthesis of **1** were carried out according to literature procedures. First, reaction of lithiated ethynyl ferrocene (**2**) with ethyl formate gave the diferrocenyl alcohol **3** [15] which was oxidised to ketone **4** [16] with activated manganese dioxide. Dibromo-olefination [15] of **4** allowed the preparation of **5**, containing the suitably functionalised ethenyl core, and subsequent Sonogashira-style [17-20] cross coupling of **5** with ethynyl ferrocene (**2**) afforded the desired tetra(ferrocenylethynyl)ethene (**1**) in 19% yield relative to **5**. Despite the high conversion observed in the preparation of **1** from **5** (crude **1** is obtained in approximately 75% yield and 80–90% purity, as assessed by ^{1}H NMR, directly from the reaction mixture) the pure compound could only be isolated in relatively low yield. Compound **1** proved to have limited stability under chromatographic conditions; however, no other method of removing the primarily ferrocene based contaminants proved successful. Thus chromatography was necessary in order to produce electrochemically and spectroscopically pure **1** despite the loss of overall yield this entailed. This instability is presumably related to the arrangement of four electron-donating ferrocene units around a highly conjugated organic core. Similarly, we have recently observed analogous instability in organic cross-conjugated systems based on an (*E*)-hexa-3-en-1,5-diyne-3,4-diyl fragment when the cross-conjugated core is substituted with four electron donating moieties [21].

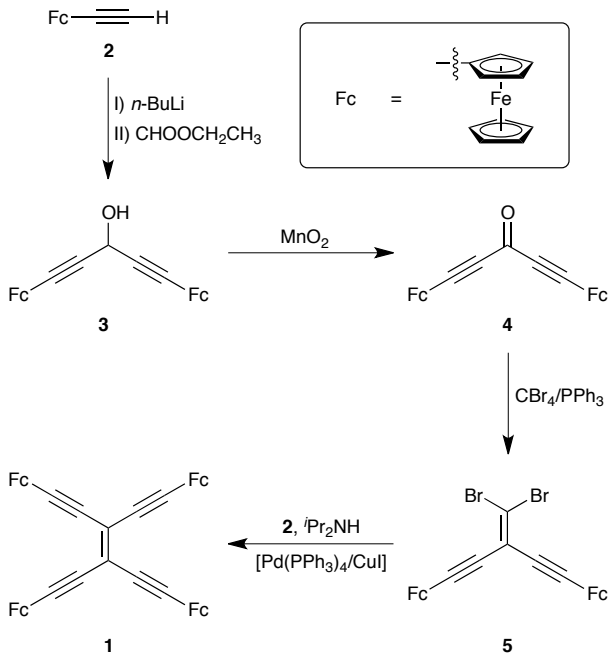

Scheme 1. Synthesis of tetra(ferrocenylethynyl)ethene.

The synthesis of **5** largely followed the methods outlined in the work of Diederich [16] and Ren [15]. While the literature methods were found to be generally efficacious, several points are worth highlighting. In this work, the MnO_2 used in the synthesis of **4** was prepared according to a method described in the early literature [22]. Commercial MnO_2 was found to react inconsistently as the properties of this compound as an oxidant are highly dependent on the particle size/surface area of the material, and this appears to vary depending on the source. In addition we note that of the two previous reports on the series of compounds **3**–**5**, only one noted successful preparation of compound **5** [15], the earlier attempt using an ostensibly identical method having failed [16]. In our hands, the literature procedure for dibromo-olefination [15] functioned perfectly well *provided* that the carbon tetrabromide used was purified by vacuum sublimation before use. Sublimation was necessary regardless of the reagent origin or age and following purification it could be stored indefinitely under nitrogen without loss of efficacy in this reaction.

2.2 Cyclic Voltammetry In dichloromethane containing 10^{-1} M NBu_4PF_6 as supporting electrolyte, a single, reversible redox process was observed in the cyclic voltammogram of compound **1** (Figure 2). This single wave has the shape of a one-electron process, indicating independent oxidation of all four ferrocenyl groups (Figure 2, Table 1). However, when $NBu_4[B\{C_6H_3(CF_3)_2\text{-}3,5\}]_4$ ($NBu_4BAr^F{}_4$) containing the weakly ion-pairing or associating anion $[BAr^F{}_4]^-$ was employed as an electrolyte, a significant separation of the individual redox events ensued, and four sequential, reversible, one-electron processes could be discerned (Figure 2, Table 1). These individual events, better resolved by differential pulse voltammetry (DPV), can be attributed to the sequential oxidation of the four ferrocenyl centres in a similar manner to other multi-ferrocenyl compounds [10-12] as outlined above, and consistent with a significant 'through-space' interaction between the ferrocenyl moieties [10,23].

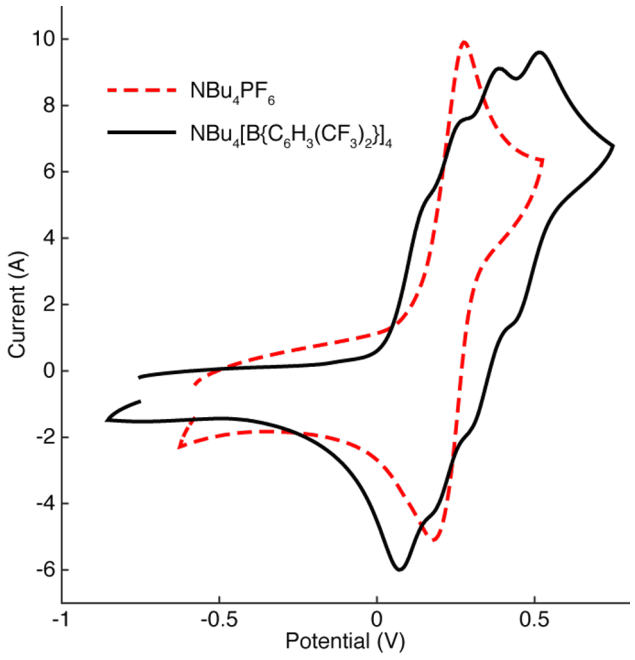

Figure 2. Cyclic voltammetry of compound **1** in CH_2Cl_2 / NBu_4PF_6 (dashed line) or CH_2Cl_2 / $NBu_4[B\{C_6H_3(CF_3)_2\text{-}3,5\}]_4$ (solid line) relative to external $FeCp_2/[FeCp_2]^+$ at 0.00 V.

Table 1. Cyclic and differential pulse voltammetry of compound **1** in CH_2Cl_2 / NBu_4PF_6 and CH_2Cl_2 / $NBu_4[B\{C_6H_3(CF_3)_2\text{-}3,5\}_4]$ relative to external $FeCp_2/[FeCp_2]^+$ at 0.00 V.

	$[X]^-$	E^0_1	E^0_2	E^0_3	E^0_4	ΔEp_1	ΔEp_2	ΔEp_3	ΔEp_4	ΔEp(ref)
1	$[PF_6]^-$	230[a]				85				80
	$[BAr^F_4]^-$	110[a]	220[a]	350[a]	480[a]	65	65	70	70	60
	$[BAr^F_4]^-$	115[b]	223[b]	343[b]	478[b]					

[a] cyclic voltammetry. [b] differential pulse voltammetry

2.3 Spectroelectrochemistry IR and UV-vis-NIR spectroelectrochemistry was carried out in CH_2Cl_2 / $NBu_4[B\{C_6H_3(CF_3)_2\text{-}3,5\}_4]$ in an attempt to spectroscopically observe each of the four redox products indicated by the individual redox waves in the voltammogram of **1** in this electrolyte. From the electrochemical data, comproportionation constants $K_c = e^{\Delta EF/RT}$, and in turn the maximum purity of the intermediate mixed-valence oxidation products at equilibrium, can be estimated as: $[\mathbf{1}]^+$ K_c = 70 (80%); $[\mathbf{1}]^{2+}$ K_c = 110 (84%); $[\mathbf{1}]^{3+}$ K_c = 190 (87%). Thus, spectra of these species will most certainly contain features from the adjacent redox partners within the comproportionated mixture.

The IR spectrum of **1** exhibits a relatively low intensity, broad ν(C≡C) band envelope with an apparent maximum at 2191 cm^{-1} and an even weaker feature near 2219 cm^{-1}. During the early stages of oxidation (comproportionated mixtures of n = 0, 1, 2) the primary ν(C≡C) band envelope gains intensity appreciably, but shifts energy only modestly to lower wavenumbers (2171 cm^{-1}). The weaker feature is less affected by oxidation. The vibrational band envelopes clearly contain multiple vibrational modes which may indicate the presence of multiple conformations in the relevant oxidation states (n = 0, 1, 2). The limited shift in frequency of these ν(C≡C) bands, coupled with increase in intensity on oxidation, likely indicates a ferrocene based oxidation event and that the initial high symmetry of **1** is lifted in the redox products. Further oxidation (n = 2, 3, 4) leads to a progressive loss of intensity in these ν(CC) bands with the band envelope shifting only slightly by ca. –3 cm^{-1} (2223 and 2168 cm^{-1}) until at the point of exhaustive electrolysis no ν(CC) bands can be discerned. The analysis is further complicated by the slow precipitation of the more highly charged species at the relatively high concentration necessary to observe the weak ν(CC) bands.

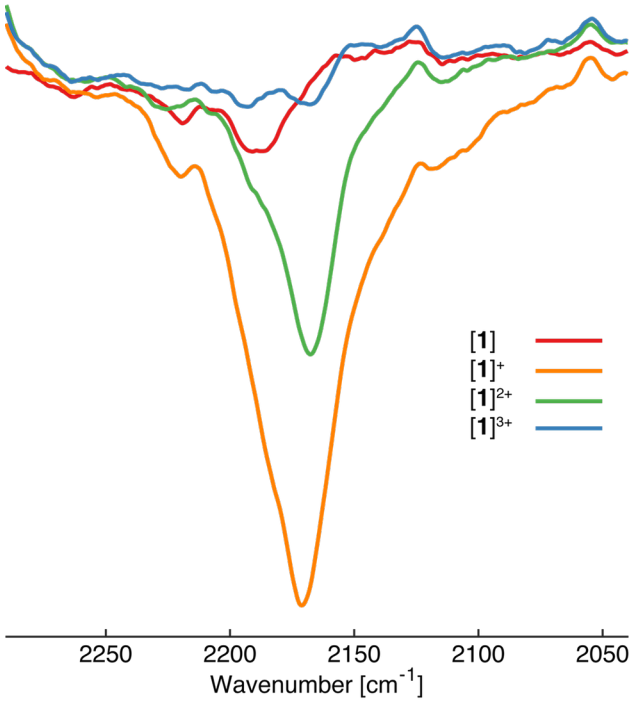

Figure 3. Reversible IR spectral changes in the ν(C≡C) region accompanying oxidation of the ferrocene moieties of **1** in CH_2Cl_2 / $NBu_4[B\{C_6H_3(CF_3)_2\text{-}3,5\}]_4$ within an OTTLE cell plotted against an arbitrary transmission scale.

Unfortunately UV-vis-NIR spectroelectrochemistry was also not particularly informative due to the heavy overlap of features in this region and the issues of comproportionation (Figure 4). The electronic absorption spectrum of neutral **1** shows characteristic absorption bands with maxima at 24750 and 19460 cm^{-1}, which are responsible for the deep purple / red colour of this compound, with no absorption features at lower energy. The broader, higher energy feature is assigned to a combination of ferrocene-to-TEE(π*) MLCT type transitions overlapped with local ferrocene transitions (Ferrocene itself absorbs at 22,540 cm^{-1}). The lower energy feature is better resolved and arises from a π-π* transition with more TEE character (See *2.4 Quantum Chemistry*).

The spectra of $[\mathbf{1}]^{n+}$ (n = 1–4) display a number of broad, heavily overlapped transitions in the visible and NIR region. The poor resolution of these multiple transitions, and complications from the comproportionation equilibria, means that meaningful deconvolution is impossible, and no clear assignments could be made. In addition to the comproportionation equilibria, as commented on above, the presence of various geometric forms arising from different relative positions of the ferrocenyl moieties 'above' and 'below' the tetraethynylethene plane (Figure 5) may lead to broadening due to the different transitions associated with each conformation. Nevertheless, at the lower concentrations used for the UV-vis-NIR work, precipitation of the higher charged species noted in the IR SEC results was less problematic and back-reduction led to almost complete recovery of the spectrum of **1**. In the absence of clear evidence for the character of the oxidized species, including assignment of any putative IVCT transition in the oxidation products, we turned to quantum chemical calculations in order to explore the molecular and electronic structure of **1** and $[\mathbf{1}]^{+}$, as a representative example of the oxidation products.

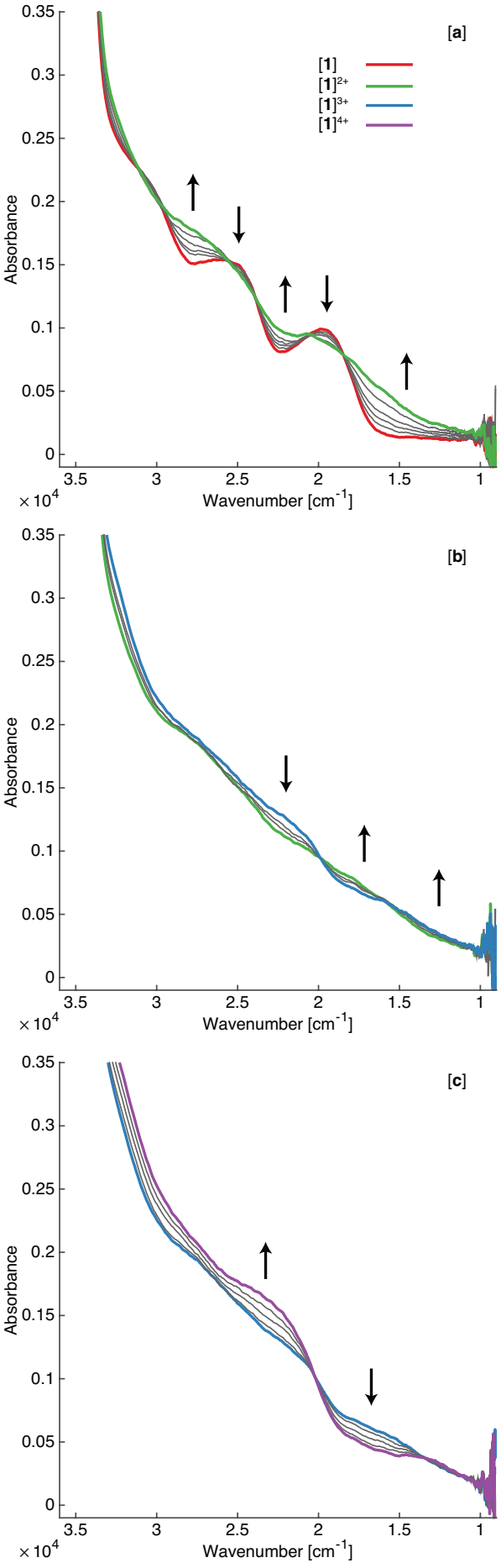
[a]
[1]
[1]2+
[1]3+
[1]4+
Absorbance
0.35
0.3
0.25
0.2
0.15
0.1
0.05
0
3.5
3
2.5
2
1.5
1
× 10^4
Wavenumber [cm^-1]
[b]
Absorbance
Wavenumber [cm^-1]
[c]
Absorbance
Wavenumber [cm^-1]

Figure 4. Reversible UV-vis-NIR spectral changes accompanying oxidation of the ferrocene moieties of **1** in CH_2Cl_2 / $NBu_4[B\{C_6H_3(CF_3)_2\text{-}3,5\}]_4$ within an OTTLE cell plotted against an arbitrary absorbance scale. (a) The unresolved oxidation of **1** to a comproportionated mixture of **1**, $[\mathbf{1}]^+$ and $[\mathbf{1}]^{2+}$. (b) Partial resolution of the further oxidation to give $[\mathbf{1}]^{3+}$. (c) Complete oxidation of the sample to $[\mathbf{1}]^{4+}$.

2.4 Quantum Chemistry To better understand the electronic structure, spectroscopic and redox properties of **1**, attention was turned to quantum chemical methods. Whilst B3LYP has been used with success to model the electronic structure of ferrocene [29], the challenges of arriving at a reliable quantum-chemical protocol for the characterisation mixed-valence compounds has been are significant [J. Hanache, O.S. Wenger, *Chem. Rev.* 2011, **111**, 5138] [A. Heckmann, C. Lambert, *Angew. Chem. Int. Ed.* 2012, **51**, 326] [C. Sutton, T. Korzdorfer, V. Coropceanu, J.-L. Bredas, *J. Phys. Chem. C*, 2014, **118**, 3925] M. Renz, K. Theilacker, C. Lambert, M. Kaupp, *J. Am. Chem. Soc.* 2009, **131**, 16292]. It has been well-established that DFT calculations with pure (local or gradient corrected) or hybrid exchange-correlation functionals such as B3LYP give an overly delocalised description due to self-interaction errors. [26] A modified form of the BLYP functional with 35% exact exchange (termed BLYP35) has been proposed as a global hybrid functional for mixed-valence compounds,[M. Renz, K. Theilacker, C. Lambert, M. Kaupp, *J. Am. Chem. Soc.* 2009, **131**, 16292] and, used in conjunction with a suitable solvent model, found to give good agreement with the available experimental data for the organic, inorganic and organometallic systems so far examined [40] [25] [M. Parthey, K.B. Vincent, M. Renz, P.A. Schauer, D.S. Yufit, J.A.K. Howard, M. Kaupp, P.J. Low, Inorg. Chem.,

53 (2014) 1544-1554] [M. Kaupp, S. Gueckel, M. Renz, S. Klawohn, K. Theilacker, M. Parthey, C. Lambert, J. Comp. Chem., 37 (2016) 93-102]

In addition to considerations of the computational methodology, it is becoming increasingly recognized that a single minimum energy structure may not model the distribution of molecular conformations present in solutions of real compounds. The idea that population of a number of local minima may impact on the appearance of spectral features has recently been discussed for several organometallic systems, including mixed-valence radical cations [24-28] [S. Scheerer, N. Rotthowe, O.S. Abdel-Rahman, X. He, S. Rigaut, H. Kvapilová, S. Záliš, R.F. Winter, Inorg. Chem. 54 (2015) 3387-3402] [J. Zhang, M.-X. Zhang, C.-F. Sun, M. Xu, F. Hartl, J. Yun, G.-A. Yu, L. Rao, S.H. Liu, Organometallics, 34 (2015) 3967-3978] [U. Pfaff, A. Hildebrandt, M. Korb, S. Oßwald, M. Linseis, K. Schreiter, S. Spange, R.F. Winter, H. Lang, Chem. Eur. J. 22 (2016) 783-801] As such DFT calculations on neutral **1** using both B3LYP-D3 and BLYP35-D3 functionals, def2-TZVP basis sets and the COSMO(CH_2Cl_2) solvent model were configured to sample a number of different orientations of the ferrocene moieties relative to each other and the plane of the tetraethynylethene moiety. In each case, the computational survey resulted in the identification of four structural minima, all lying very close in energy to one another (Figure 5). Given the similarity of results for **1** from each functional, and the more appropriate level of exact exchange in BLYP35 for the study of the redox products, the discussion of the electronic structure of **1** which follows is restricted to results from BLYP35-D3/def2-TZVP/COSMO(CH_2Cl_2) for brevity.

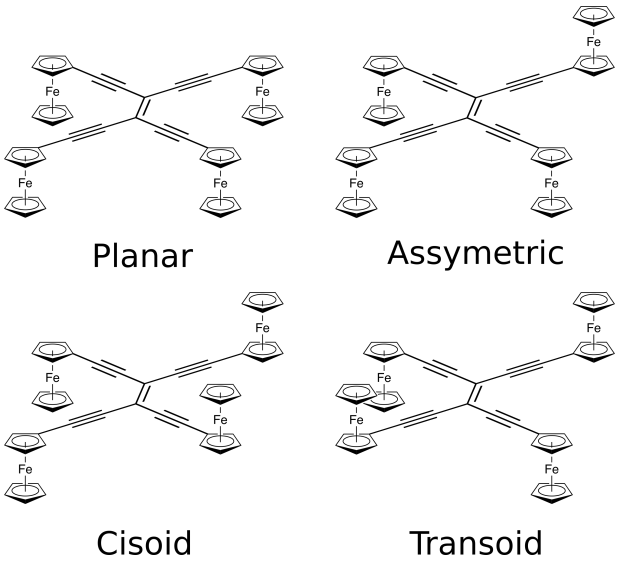

Figure 4. A representation of the structures of the four initial conformers used in the quantum chemical investigation of **1**.

Table 2. Energies of the BLYP35-D3/def2-TZVP/COSMO(CH_2Cl_2) optimised structures in kJ mol^{-1} for [**1**] and $[\mathbf{1}]^+$ relative to the energetically most favourable conformer.

	[**1**]	$[\mathbf{1}]^+$
Planar	0.00	0.00
Asymmetric	2.29	4.65
Cisoid	0.06	1.59
Transoid	4.72	5.81

Optimisation of the four initial structures of $[\mathbf{1}]^{n+}$ (n = 0, 1) at the BLYP35-D3/def2-TZVP/COSMO(CH_2Cl_2) level predicts the "planar" structure (all ferrocenyl moieties co-located on the same face of the tetraethynylethene ligand) to be energetically most favourable, not only in case of the neutral compound (n = 0) but also for the cation (n

= 1). However, in each case (n = 0, 1) the energies of the different conformers differ little (Table 2). The $[C_5H_4]^-$ ligands of individual ferrocene moieties, which are staggered with respect to the corresponding C_5H_5 ligand, do not lie in the plane of the tetraethynylethene fragment. Rather, the ferrocenyl groups are arranged in a propeller-like fashion, presumably in order to minimise steric interactions (Figure 6). The barrier for rotation of one Fc unit by 180 degrees is estimated to be ~15 kJ mol^{-1} (from calculations which identify the transition state to be an intermediate geometry in which the mobile ferrocene moiety lies approximately perpendicular to the other ferrocene fragments and in plane with the tetraethynylethene backbone). Therefore, a dynamic equilibrium between conformers appears likely in solution at room temperature.

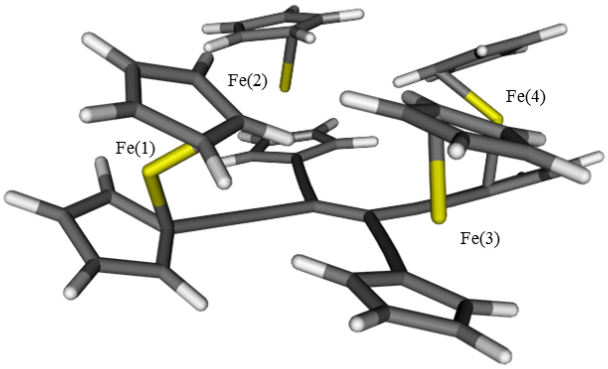

Figure 6. Planar conformer of [**1**] optimised at BLYP35-D3/def2-TZVP/COSMO(DCM) level.

An average Fe–Cp(centroid) distance of 1.70 Å is obtained for all neutral conformers. This compares with data for the optimised structure of FcH under the same conditions (Fe–Cp(centroid) = 1.69 Å) though the computational model overestimates this distance by ca. 0.04 Å (FcH experimental (XRD) data Fe–Cp(centroid) = 1.65 Å [30]). Oxidation to $[\mathbf{1}]^+$ leads to elongation of the Fe–Cp(centroid) distances to 1.74 Å

for just one ferrocenyl moiety with all other interatomic distances virtually unchanged, strongly suggesting a description of $[\mathbf{1}]^+$ in terms of a localised (class I) or weakly coupled (class II) mixed-valence system is appropriate.

The compositions of the highest occupied molecular orbitals (HOMO) and lowest unoccupied molecular orbitals (LUMO) of the neutral isomers are shown in Table 3. On average the HOMO and LUMO have only small metal contributions of 16 % and 9 %, respectively. Differences between the conformers in terms of the contribution and distribution of the metallic contribution to these frontier orbitals are negligible. For each conformer, the HOMO and LUMO are better described in terms of the π-system of the tetraethynylethene backbone (Table 3). Occupied orbitals with more substantial metal character lie at lower energy (e.g. planar-**1**: HOMO-4 (Fe 89.5%); HOMO-3 (Fe 88.1%); HOMO-2 (Fe 85.6%); HOMO-1 (Fe 77.9%), selected examples of which are shown in Figure 7.

Table 3: Percentage contribution of the metal centres and the tetraethynylethene backbone (TEE) to the frontier molecular orbitals of the different conformers of neutral [**1**].

	Fe(1)	Fe(2)	Fe(3)	Fe(4)	Total Fe	TEE
Planar						
HOMO	3.7	4.4	4.4	3.7	16.3	60.4
LUMO	2.0	2.4	2.4	2.0	8.8	76.6
Asymmetric						
HOMO	4.3	3.9	3.9	4.0	16.2	60.6
LUMO	2.4	2.1	2.1	2.1	8.7	76.6
Cisoid						
HOMO	4.0	3.8	4.2	4.3	16.4	60.4
LUMO	2.0	1.9	2.4	2.5	8.8	76.6
Transoid						
HOMO	4.0	4.0	4.1	4.0	16.1	60.7
LUMO	2.2	2.2	2.2	2.2	8.8	76.5

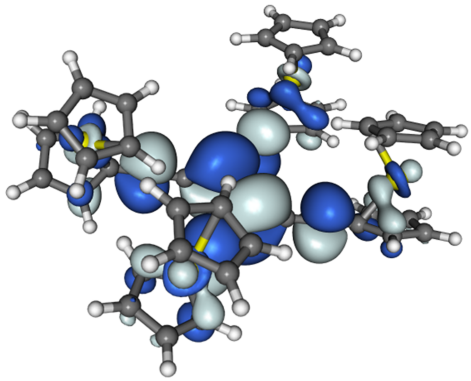

LUMO [**1**]

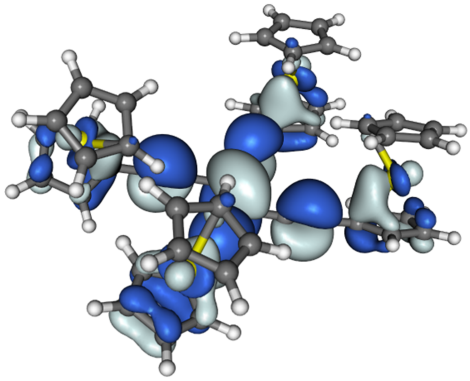

HOMO [**1**]

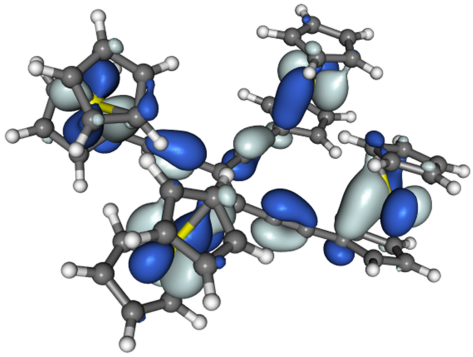

HOMO-1 [**1**]

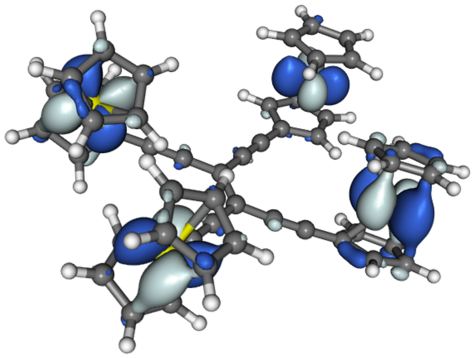

HOMO-3 [**1**]

Figure 7: Selected frontier orbitals of planar-**1** (isosurfaces ±0.02 (e/bohr^3)$^{1/2}$).

Time-dependent DFT (TD DFT) calculations performed on the lowest energy ('planar') conformer of **1** indicates the first electronic transition of significant oscillator strength (calculated 22,840 cm^{-1}; observed 19790 cm^{-1}) corresponds to the HOMO-LUMO transition, which has significant TEE π-π* character (Table 3, Figure 7). The higher energy absorption envelopes observed in the experimental spectrum with an apparent maxima at 25640 cm^{-1} and a shoulder at 30340 cm^{-1} correspond to electronic transitions from HOMO-1 and HOMO-3 to LUMO (calculated 29861 cm^{-1}) and HOMO-3 → LUMO (calculated 30774 cm^{-1}) both of which have ferrocene-TEE MLCT character; the ferrocene localised transitions are also likely within these envelopes (c.f. Ferrocene 22540, 30550 cm^{-1}).

In the case of the oxidised species [**1**]$^+$ there is significant orbital re-ordering, and the frontier molecular orbitals of all conformers exhibit a considerable degree of localisation on one ferrocenyl moiety (Table 4, Figure 8). The LUMO and in particular SOMO now exhibit appreciable localisation on the oxidised metal centre (Fe(2)), in clear support of a localised MV radical cation. The tetraethynylethene π-system which comprises the HOMO in **1** descends below the SOMO in [**1**]$^+$ and forms the first doubly occupied HOMO with only slightly more metal character than the HOMO of the neutral complexes (cf. Table 3).

Table 4. Percentage metal and TEE backbone contributions to the frontier molecular orbitals of the four conformers of the radical cation $[\mathbf{1}]^{+}$.

					Total	TEE
	Fe(1)	Fe(2)	Fe(3)	Fe(4)	Fe	
Planar						
HOMO	8.0	1.5	5.4	3.5	18.3	57.4
SOMO	0.2	46.8	0.9	0.7	48.6	25.9
LUMO	1.4	30.4	1.5	1.3	34.7	50.1
Asymmetric						
HOMO	8.7	1.3	4.9	3.8	18.7	57.0
SOMO	0.2	50.0	0.7	0.6	51.5	23.4
LUMO	1.6	27.3	1.4	1.5	31.8	52.6
Cisoid						
HOMO	8.1	1.3	5.3	4.0	18.6	57.2
SOMO	0.2	50.5	0.7	0.7	52.1	22.4
LUMO	1.5	25.6	1.6	1.8	30.4	54.4
Transoid						
HOMO	8.4	1.4	5.0	3.8	18.6	57.1
SOMO	0.2	48.9	0.8	0.7	50.6	23.9
LUMO	1.5	27.9	1.5	1.5	32.4	52.8

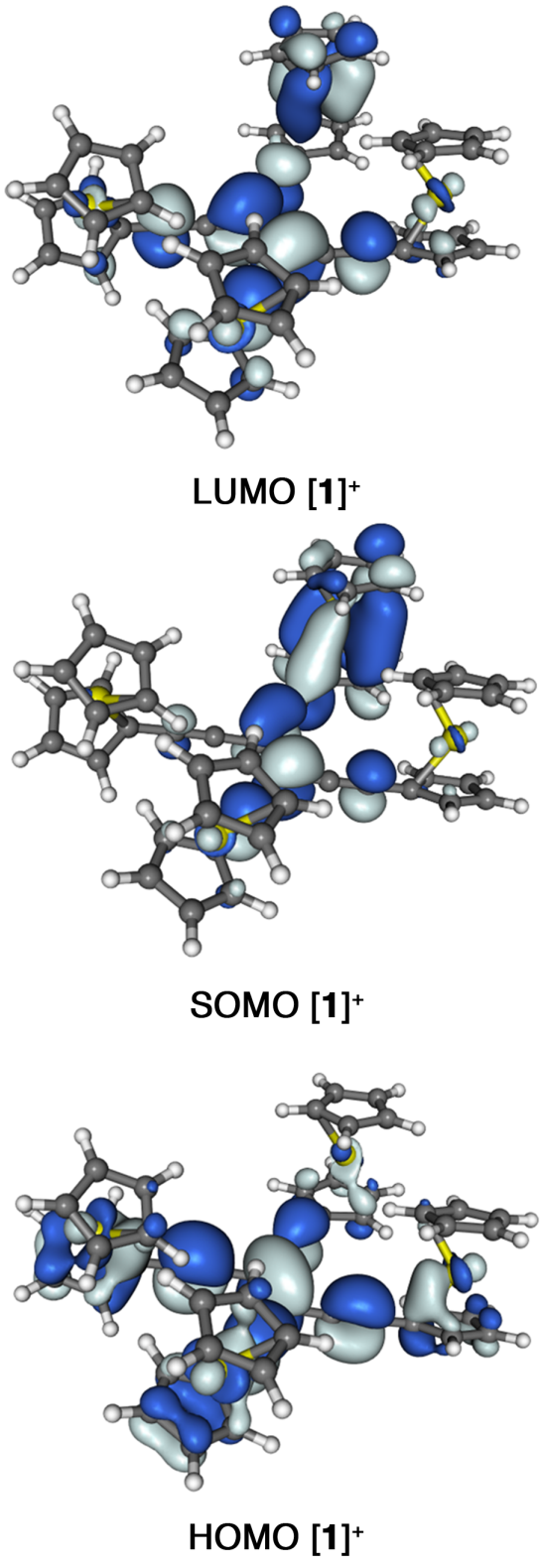

Figure 8. LUMO (upper), SOMO (middle), and HOMO (lower) of planar-[**1**]$^{+}$ (±0.02 (e/bohr^{3})$^{1/2}$).

3. CONCLUSION

The multi-ferrocenyl compound tetra(ferrocenylethynyl)ethene (**1**) has been prepared and isolated. Comparisons of cyclic voltammetry experiments with **1** conducted in dichloromethane solutions containing NBu_4PF_6 and $NBu_4BAr^F{}_4$ electrolytes indicate that there is a significant through-space contribution to the separation of the four redox waves observed in the latter, more weakly associating, electrolyte. UV-vis-NIR and IR spectroelectrochemical experiments conducted in dichloromethane / 0.1 M $NBu_4BAr^F{}_4$ also reveal five individual redox states ($[\mathbf{1}]^{n+}$ (n = 0 – 4), although analyses of data from the redox products were complicated by low intensity (IR) and heavily overlapping (UV-vis-NIR) electronic transitions and comproportionation equilibria. Nevertheless these spectroelectrochemical data are strongly suggestive of a localised ferrocinium oxidation.

Quantum chemical calculations using the BLYP35 functional, large basis set and solvent model indicate that the frontier orbitals of the parent compound **1** are closely related to the π-system of tetraethynylethene, supported by small contributions from the ferrocene metal centers, the ferrocene-type fragment orbitals lying lower in energy. On oxidation to $[\mathbf{1}]^+$, orbital re-ordering takes place, giving a system well described in terms of a localized ferrocene oxidation, fully consistent with the suggestions made on the basis of the spectroelectrochemical experiments. Further challenges for this work now rest on taking the design concept towards a more tractable and easily characterised analogue for further study in the higher charge states.

4. EXPERIMENTAL

4.1 General Conditions All reactions were carried out under an atmosphere of dry nitrogen using standard Schlenk techniques. Diisopropylamine was distilled over calcium sulfate and freeze-pump-thaw degassed before use, other solvents were standard reagent grade and used as received. No special precautions were taken to exclude air or moisture during workup except where otherwise indicated. Ethynyl ferrocene (**1**) was synthesised according to ref [31] or [32]. The compounds **3** [15], **4** [16], **5** [15], MnO_2 [22], $NBu_4[B\{C_6H_3(CF_3)_2\text{-}3,5\}]_4$ [33] and $[Pd(PPh_3)_4]$ [34] were synthesised according to literature procedures, and CBr_4 was sublimed before use. All other reagents were commercially available and used as received. NMR spectra were recorded at 23 ºC on a Varian NMR Systems 600 (^{1}H, 599.8 MHz; ^{13}C, 150.8 MHz) spectrometer using $CDCl_3$ as the solvent. Chemical shifts were determined relative to internal solvent signals [8]. Assignment of the ^{1}H and ^{13}C NMR data was supported by gradient selected ^{13}C,^{1}H HMQC and HMBC experiments. IR spectra were recorded on a Nicolet Avatar 6700 FT-IR from samples in dichloromethane using a CaF_2 cell. ASAP-MS spectra were recorded from solid samples on an LCT Premier XE mass spectrometer (Waters Ltd., U.K.) or Xevo QToF mass spectrometer (Waters Ltd., U.K.). Cyclic voltammetry was carried out using a Palm Instruments EmStat2 potentiostat, with a platinum disc working electrode, a platinum wire counter electrode, and a platinum wire pseudo-reference electrode, from solutions in dichloromethane containing either 10^{-1} M NBu_4PF_6 or 10^{-1} M $NBu_4[B\{C_6H_3(CF_3)_2\text{-}3,5\}]_4$ as the electrolyte. Measurements with $\nu = 100$, 200, 400 and 800 $mV.s^{-1}$ showed that the ratio of the anodic to cathodic peak currents varied linearly as a function of the square root of scan rate in all cases. The decamethylferrocene/decamethylferrocenium ($FeCp^*_2/[FeCp^*_2]^+$) couple was used as

an internal reference for potential measurements such that the couple falls at –0.55 V (CH_2Cl_2 / NBu_4PF_6) or –0.62 V (CH_2Cl_2 / $NBu_4[B\{C_6H_3(CF_3)_2\text{-}3,5\}]_4$) relative to external $FeCp_2/[FeCp_2]^+$ at 0.00 V [35]. ATR-IR and UV-vis-NIR spectra were recorded on a Bruker Vertex 70v FT-IR spectrometer and a Scinco S3100 diode array spectrophotometer, respectively. Spectroelectrochemical experiments at room temperature were conducted with an OTTLE [36] cell equipped with a Pt-minigrid working electrode and CaF_2 windows. The optical path of the cell was ca. 0.2 mm. The concentrations of the analytes and the supporting electrolyte used in these measurements were 1.3×10^{-2} and 3×10^{-1} mol dm^{-3} for IR, and 10^{-3} and 3×10^{-1} mol dm^{-3} for the UV-vis-NIR studies, respectively.

*4.2. Preparation of $(FcC{\equiv}C)_2C{=}C(C{\equiv}CFc)_2$ (**1**)*

Compound **2** (62.8 mg, 299 μmol), **5** (60.0 mg, 100 μmol), $[Pd(PPh_3)_4]$ (5.76 mg, 4.98 μmol) and Cu(I)I (1.90 mg, 9.97 μmol) were added to diisopropylamine (20 mL) and the mixture was stirred at room temperature for 16 h. The reaction mixture was filtered and the precipitate was extracted in to hexanes/dichloromethane (50:50 (v/v)). Following removal of the solvents, the residue was taken up in dichloromethene and purified by column chromatography (eluent: hexanes → hexanes/dichloromethane (70:30 (v/v))) carefully eluting three close running bands. The solvent was removed from the third band (rf = 0.35 in hexanes/dichloromethane (70:30 (v/v))) to afford **1** in 19% yield (16.0 mg, 18.6 μmol) as a dark purple solid. ^{1}H NMR (599.7 MHz, $CDCl_3$): δ 4.28 (s, 20H, C_5H_5), 4.30 (m, 8H, H2/H5 C_5H_4), 4.59 (m, 8H, H3/H4 C_5H_4). ^{13}C NMR (150.8 MHz, $CDCl_3$): δ 64.9 (C1 C_5H_4), 69.6 (C3/C4 C_5H_4), 70.5 (C_5H_5), 71.9 (C2/C5 C_5H_4), 85.0 (C=C–*C*≡C), 97.7 (C=C–C≡*C*), 110.2 (*C*=C–C≡C).

ASAP-MS(+): m/z 861.1 $[M]^+$. ASAP-HRMS(+) m/z: 860.0228 (found); 860.0215 (calculated for $C_{50}H_{36}Fe_4$)

4.3 Quantum Chemical Methods Structure optimizations as well as bonding analyses were performed using a version of the TURBOMOLE 6.4 [37] code locally modified by the Berlin group. All DFT calculations reported in the paper were performed with the global hybrid functional BLYP35 [26,38-40]. This exchange-correlation functional was constructed according to

$$E_{XC} = 0.65(E_X^{LDSA} + \Delta E_X^{B88}) + 0.35E_X^{exact} + E_C^{LYP}.$$

While not a thermochemically optimized functional, BLYP35 has been shown to provide good agreement with ground- and excited-state experimental data for organic mixed-valence systems, [38-42] as well as for mixed-valence transition-metal complexes [24-26]. Since all experiments were carried out in dichloromethane (permittivity ε = 8.93), it has been modeled by the conductor-like screening solvent model (COSMO) [43]. Semiempirical dispersion correction terms within Grimme's DFT-D3 approach [44] were added, as implemented in TBM 6.4 [45]. For all calculations Triple-zeta basis sets (def2-TZVP) were used with grid size m3 (grid 1 for the SCF and grid 3 for the final energy evaluation) [46]. Spin-density isosurface plots were obtained with the Molekel program [47].

5. ACKNOWLEDGEMENTS

We gratefully acknowledge funding from the EPSRC, ARC (DP 140100855) and DFG (KA1187/13-1). PJL held an EPSRC Leadership Fellowship and now holds an ARC Future Fellowship (FT 120100073). This project has been greatly enhanced by

funding from the DAAD/Go8 enabling exchange visits of JBGG, SG, PJL and MK between Perth and Berlin. FH thanks EPSRC for funding (EP/K00753X) and the University of Reading for the support of the Reading Spectroelectrochemistry laboratory (Project D14-015).

6. REFERENCES

[1] C.S. Lent, Science 288 (2000) 1597–1599.
[2] A. Pulimeno, M. Graziano, A. Sanginario, V. Cauda, D. Demarchi, G. Piccinini, IEEE Trans. Nanotechnology 12 (n.d.) 498–507.
[3] J.A. Christie, R.P. Forrest, S.A. Corcelli, N.A. Wasio, R.C. Quardokus, R. Brown, S.A. Kandel, Y. Lu, C.S. Lent, K.W. Henderson, Angewandte Chemie 127 (2015) 15668–15671.
[4] Z. Li, T.P. Fehlner, Inorg. Chem. 42 (2003) 5715–5721.
[5] H. Qi, S. Sharma, Z. Li, G.L. Snider, A.O. Orlov, C.S. Lent, T.P. Fehlner, J. Am. Chem. Soc. 125 (2003) 15250–15259.
[6] J. Jiao, G.J. Long, F. Grandjean, A.M. Beatty, T.P. Fehlner, J. Am. Chem. Soc. 125 (2003) 7522–7523.
[7] D. Astruc, Electron Transfer and Radical Processes in Transition-Metal Chemistry, Weily-VCH, Weinheim, 1995.
[8] G.R. Fulmer, A.J.M. Miller, N.H. Sherden, H.E. Gottlieb, A. Nudelman, B.M. Stoltz, J.E. Bercaw, K.I. Goldberg, Organometallics 29 (2010) 2176–2179.
[9] H. Fink, N.J. Long, A.J. Martin, G. Opromolla, A. White, D.J. Williams, P. Zanello, Organometallics 16 (1997) 2646–2650.
[10] F. Barrière, N. Camire, W.E. Geiger, U.T. Mueller-Westerhoff, R. Sanders, J. Am. Chem. Soc. 124 (2002) 7262–7263.
[11] A.K. Diallo, J.-C. Daran, F. Varret, J. Ruiz, D. Astruc, Angew. Chem. Int. Ed. 48 (2009) 3141–3145.
[12] A.K. Diallo, C. Absalon, J. Ruiz, D. Astruc, J. Am. Chem. Soc. 133 (2011) 629–641.
[13] O.F. Koentjoro, P. Zuber, H. Puschmann, A.E. Goeta, J.A.K. Howard, P.J. Low, Journal of Organometallic Chemistry 670 (2003) 178–187.
[14] R.R. Tykwinski, M. Schreiber, R.P. Carlon, F. Diederich, V. Gramlich, Helvetica Chimica Acta 79 (1996) 2249–2281.
[15] G.-L. Xu, B. Xi, J.B. Updegraff, J.D. Protasiewicz, T. Ren, Organometallics 25 (2006) 5213–5215.
[16] A. Auffrant, F. Diederich, C. Boudon, J.P. Gisselbrecht, M. Gross, Helvetica Chimica Acta 87 (2004) 3085–3105.
[17] K. Sonogashira, Y. Tohda, N. Hagihara, Tetrahedron Lett. 50 (1975) 4464–4470.
[18] K. Sonogashira, Y. Tohda, N. Hagihara, Tetrahedron Lett. 16 (1975) 4467–4470.

[19] K. Sonogashira, J. Organomet. Chem. 653 (2002) 46–49.
[20] R. Chinchilla, C. Najera, Chem. Rev. 107 (2007) 874–922.
[21] J.B.G. Gluyas, V. Manici, S. Gückel, K.B. Vincent, D.S. Yufit, J.A.K. Howard, B.W. Skelton, A. Beeby, M. Kaupp, P.J. Low, The Journal of Organic Chemistry (2015) acs.joc.5b02240.
[22] J. Attenburrow, A.F.B. Cameron, J.H. Chapman, R.M. Evans, B.A. Hems, A.B.A. Jansen, T. Walker, Journal of the Chemical Society (Resumed) (1952) 1094.
[23] F. Barrière, W.E. Geiger, J. Am. Chem. Soc. 128 (2006) 3980–3989.
[24] M. Parthey, J.B.G. Gluyas, P.A. Schauer, D.S. Yufit, J.A.K. Howard, M. Kaupp, P.J. Low, Chem. Eur. J. 19 (2013) 9780–9784.
[25] M. Parthey, J.B.G. Gluyas, M.A. Fox, P.J. Low, M. Kaupp, Chem. Eur. J. 20 (2014) 6895–6908.
[26] M. Parthey, M. Kaupp, Chem. Soc. Rev. 43 (2014) 5067–5088.
[27] S.W. Lehrich, A. Hildebrandt, T. Rüffer, M. Korb, P.J. Low, H. Lang, Organometallics 33 (2014) 4836–4845.
[28] U. Pfaff, A. Hildebrandt, M. Korb, D. Schaarschmidt, M. Rosenkranz, A. Popov, H. Lang, Organometallics (2015) 2826–2840.
[29] S. Coriani, A. Haaland, T. Helgaker, P. Jørgensen, ChemPhysChem 7 (2006) 245–249.
[30] P. Seiler, J.D. Dunitz, Acta Crystallographica B35 (1979) 2020–2032.
[31] D. Courtney, C.J. McAdam, A.R. Manning, H. Müller-Bunz, Y. Ortin, J. Simpson, Journal of Organometallic Chemistry 705 (2012) 7–22.
[32] J. Polin, H. Schottenberger, Organic Syntheses 73 (1996) 262.
[33] N.A. Yakelis, R.G. Bergman, Organometallics 24 (2005) 3579–3581.
[34] S.O. Mihigo, W. Mammo, M. Bezabih, K. Andrae-Marobela, B.M. Abegaz, Bioorg. Med. Chem. 18 (2010) 2464–2473.
[35] J.B.G. Gluyas, A.J. Boden, S.G. Eaves, H. Yu, P.J. Low, Dalton Trans. 43 (2014) 6291–6294.
[36] M. Krejčik, M. Daněk, F.J. Hartl, J. Electroanal. Chem. 317 (1991) 179–187.
[37] TURBOMOLE; Turbomole GmbH: A development of University of Karlsruhe and Forschungszentrum Karlsruhe GmbH: Karlsruhe, Germany, 1989−2007, 2012.
[38] M. Kaupp, M. Renz, M. Parthey, M. Stolte, F. Würthner, C. Lambert, Phys. Chem. Chem. Phys. 13 (2011) 16973.
[39] M. Renz, K. Theilacker, C. Lambert, M. Kaupp, J. Am. Chem. Soc. 131 (2009) 16292–16302.
[40] M. Renz, M. Kess, M. Diedenhofen, A. Klamt, M. Kaupp, J. Chem. Theory Comput. 8 (2012) 4189–4203.
[41] M. Renz, M. Kaupp, J. Phys. Chem. A 116 (2012) 10629–10637.
[42] S.F. Völker, M. Renz, M. Kaupp, C. Lambert, Chem. Eur. J. 17 (2011) 14147–14163.
[43] A. Klamt, G. Schüürmann, J. Chem. Soc., Perkin Trans. 2 (1993) 799.
[44] S. Grimme, Chem. Eur. J. 10 (2004) 3423–3429.
[45] S. Grimme, J. Antony, S. Ehrlich, H. Krieg, J. Chem. Phys. 132 (2010) 154104.
[46] F. Weigend, M. Häser, H. Patzelt, R. Ahlrichs, Chem. Phys. Lett. 294 (1998) 143–152.
[47] U. Varetto, MOLEKEL 5.4; Swiss National Computing Centre, Manno, Switzerland.

FOR TABLE OF CONTENTS/GRAPHICAL ABSTRACT USE ONLY

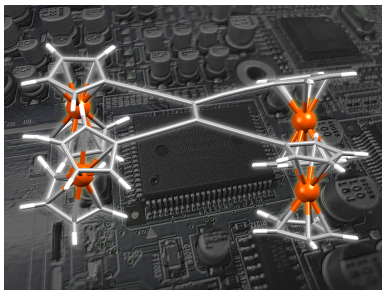

Image background modified from https://flic.kr/p/e6YtfG with permission.

Tetra(ferrocenylethynyl)ethane (**1**) has been prepared in four steps from ethynyl ferrocene. Four individual redox processes could be resolved by selection of an appropriate non-coordinating electrolyte. Spectroelectro- and quantum-chemical investigations of the monocation $[\mathbf{1}]^{+}$ suggested charge localisation to single ferrocene moiety occurs on oxidation.